Bull. Mater. Sci., Vol. 32, No. 3, June 2009, pp. 313–319. © Indian Academy of Sciences.

Compatibility of RuO_2 electrodes with PZT ceramics

K T JACOB*, G RAJITHA and V S SAJI

Department of Materials Engineering, Indian Institute of Science, Bangalore 560 012, India

Abstract. **Because of its high electrical conductivity and good diffusion barrier properties ruthenium dioxide (RuO_2) is a good electrode material for use with ferroelectric lead zirconate–titanate (PZT) solid solutions. Under certain conditions, RuO_2 can react with PZT to form lead ruthenate ($Pb_2Ru_2O_{6.5}$) during processing at elevated temperatures resulting in lead depletion from PZT. The standard Gibbs energies of formation of RuO_2 and $Pb_2Ru_2O_{6.5}$ and activities of components of the PZT solid solution have been determined recently. Using this data along with older thermodynamic information on $PbZrO_3$ and $PbTiO_3$, the stability domain of $Pb_2Ru_2O_{6.5}$ is computed as a function of PZT composition, temperature and oxygen partial pressure in the gas phase. The results show $PbZrO_3$-rich compositions are more prone to react with RuO_2 at all temperatures. Increasing temperature and decreasing oxygen partial pressure suppress the reaction. Graphically displayed are the reaction zones as a function of oxygen partial pressure and PZT composition at temperatures 973, 1173 and 1373 K.**

Keywords. **$Pb_2Ru_2O_{6.5}$ formation; RuO_2 electrode; $Pb(Zr_xTi_{1-x})O_3$ (PZT) solid solution; thermodynamic analysis; interface reactions; stability fields.**

1. Introduction

Ferroelectric ceramic materials based on the solid solution $Pb(Zr_xTi_{1-x})O_3$ (PZT) are used in sensors, actuators, electromechanical transducers, MEMS devices and high-density nonvolatile memories (ferroelectric random access memory). Main advantages of PZT solid solutions are their relatively low annealing temperatures (773–873 K) compatible with semiconductor processing, and high remanent polarization. In the development of thin film ferroelectric devices electrodes play an important role in determining the device properties and performance. Platinum (Pt) is currently used as bottom electrode for lead zirconate titanate (PZT) thin films (Kim *et al* 1997). However, Pt bottom electrodes are associated with polarization fatigue after repeated switching cycles (Taylor *et al* 1995). The use of conducting oxides such as RuO_2, IrO_2 and $(La,Sr)CoO_3$ improves fatigue properties (Al-shareef *et al* 1995; Law *et al* 1999). Oxide electrodes inhibit fatigue primarily by acting as sinks for oxygen vacancies. However, these oxide electrodes are associated with higher leakage current and greater susceptibility to dielectric breakdown. PZT films on Pt electrodes exhibit strong crystallographic orientation with prominent (101) peaks in XRD. However, when RuO_2 is used as bottom electrode for PZT thin films, several peaks corresponding to (111), (200) and (211) planes of PZT are present. These planes contain more defect states than the (101) plane, causing higher leakage current than with Pt bottom electrode (Park *et al* 1999). The high leakage current and lower remanent polarization observed with RuO_2 electrodes in some cases was attributed to the possible formation of conducting lead ruthenate (PRO) with pyrochlore structure (Kim *et al* 1999). Bencan *et al* (2001) reported the formation of $Pb_2Ru_2O_{6.5}$ by the reaction of RuO_2 with PZT at 1223 K. Taking advantage of this reaction, PRO/Pt hybrid electrodes can be developed to overcome the difficulties encountered with RuO_2/Pt hybrids. Seong *et al* (2004) have shown that 35 nm PRO inter-layers inserted between Pt and PZT play an important role in improving the ferroelectric properties of PZT thin films for nonvolatile memory device application. Presented in this paper is a thermodynamic analysis of the reaction between PZT and RuO_2 as a function of temperature, oxygen partial pressure and PZT composition. The results are presented in the form of stability field diagrams, showing reaction and no-reaction zones, which help in optimizing the processing window for various devices.

2. Review of literature

Reviewed and compiled in this section are essential information required for assessing the interaction between RuO_2 and lead zirconate–titanate (PZT) solid solutions. Phase diagrams of the component ternary systems provide a visual summary of compatibility relations. Thermodynamic data provide the input for the calculations.

2.1 *Phase relations*

The subsolidus phase diagrams for the system PbO–RuO_2–TiO_2 given by Hrovat *et al* (1994) and Jacob and

*Author for correspondence (katob@materials.iisc.ernet.in)

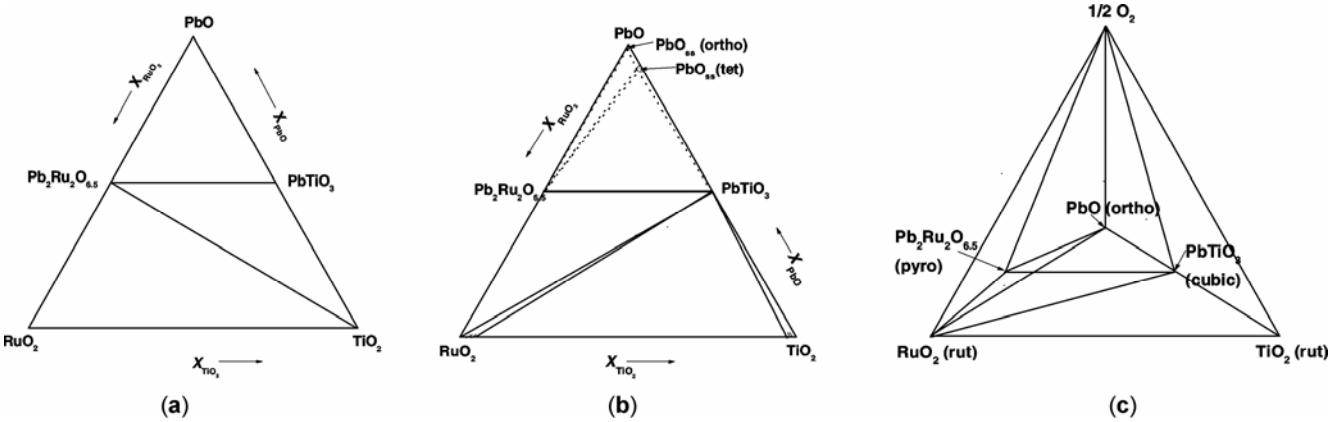

Figure 1. (**a**) The subsolidus phase diagram of the ternary system PbO–RuO_2–TiO_2 in air proposed by Hrovat *et al* (1994), (**b**) projection of phase equilibria in the quaternary PbO–RuO_2–TiO_2–O_2 on to the ternary triangle PbO–RuO_2–TiO_2, and (**c**) quaternary system PbO–RuO_2–TiO_2–O_2 proposed by Jacob and Subramanian (2007) at 1123 K.

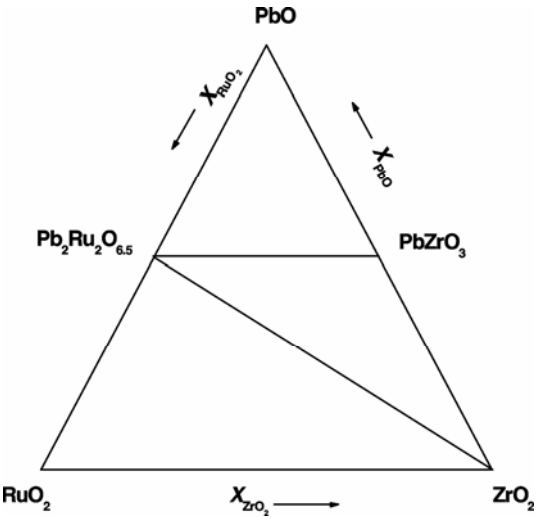

Figure 2. The phase diagram of the ternary system PbO–RuO_2–ZrO_2 proposed by Bencan *et al* (2001) at 1223 K.

Subramanian (2007) are shown in figure 1. According to Hrovat *et al* (1994), the tie-lines are between TiO_2 and $Pb_2Ru_2O_{6.5}$ and between $PbTiO_3$ and $Pb_2Ru_2O_{6.5}$ in air. Their phase diagram, shown as figure 1(a), indicates that TiO_2 will not react with $Pb_2Ru_2O_{6.5}$. However, Jacob and Subramanian (2007) showed that long exposure of an equimolar mixture of TiO_2 and $Pb_2Ru_2O_{6.5}$ at 1123 K resulted in the formation of $PbTiO_3$ and RuO_2, suggesting that the phase relations suggested by Hrovat *et al* (1994) are incorrect. Through thermodynamic calculations they proposed a phase diagram at 1123 K shown as figure 1(b); the correct tie-lines are between $PbTiO_3$ and RuO_2 and between $Pb_2Ru_2O_{6.5}$ and $PbTiO_3$. Thus, RuO_2 will not react with $PbTiO_3$. There is negligible solid solubility of RuO_2 in $PbTiO_3$. Jacob and Subramanian (2007) pointed out that the $Pb_2Ru_2O_{6.5}$ compound does not belong strictly to the binary system PbO–RuO_2 since it contains excess oxygen. They proposed the phase diagram of the quaternary system PbO–RuO_2–TiO_2–O_2 shown as figure 1(c). Figure 1(b) is the projection of quaternary phase relations from the oxygen apex onto the base triangle.

Bencan *et al* (2001) studied the subsolidus phase equilibria of the RuO_2–PbO–ZrO_2 fired at 1223 K in air. Their proposed tie lines are between $Pb_2Ru_2O_{6.5}$ and ZrO_2 and between $Pb_2Ru_2O_{6.5}$ and $PbZrO_3$ as shown in figure 2. This diagram is consistent with thermodynamic data and indicates that RuO_2 will react with $PbZrO_3$ to form $Pb_2Ru_2O_{6.5}$ and ZrO_2. There is negligible solid solubility of RuO_2 in ZrO_2.

Hrovat *et al* (2001) showed that in air there are no compounds or solid solutions in the system RuO_2–TiO_2–ZrO_2, either along the binary edges or inside the ternary triangle at 1223 K. However, Jacob *et al* (2006) have shown that an interoxide compound $ZrTiO_4$ is present in the binary system TiO_2–ZrO_2 at 1373 K.

Displayed in figure 3 is an isothermal section of the phase diagram for the system PbO–TiO_2–ZrO_2 at 1373 K suggested recently by Jacob and Rannesh (2007). The tie-lines from the PZT solid solution are skewed towards the ZrO_2-rich solid solution: only the $PbTiO_3$-rich compositions are in equilibrium with TiO_2 solid solution and $ZrTiO_4$.

2.2 *Thermodynamic data for compounds and solid solutions*

Based on new solid-state electrochemical measurements, Jacob *et al* (2000a) refined thermodynamic data for RuO_2. The standard Gibbs energy of formation of RuO_2 from Ru and O_2 over the temperature range from 900 to 1200 K is given by

$$\mathrm{Ru}(hcp) + \mathrm{O_2}(g) \rightarrow \mathrm{RuO_2\ (rut)}, \quad (1)$$

$$\Delta G_1^0(\pm 80)/\mathrm{J\ mol^{-1}} = -324720 + 354{\cdot}21T - 23{\cdot}490T\ln T. \quad (2)$$

Jacob and Shim (1981) determined the standard Gibbs energy of formation of $PbZrO_3$ from yellow PbO with orthorhombic structure and ZrO_2 with monoclinic structure in the temperature range from 800–1400 K using the solid-state electrochemical technique. For the reaction,

$$PbO\ (ortho) + ZrO_2\ (mono) \rightarrow PbZrO_3\ (cubic), \quad (3)$$

$$\Delta G_3^0(\pm 800)/\text{J mol}^{-1} = -4540 - 6{\cdot}76T. \quad (4)$$

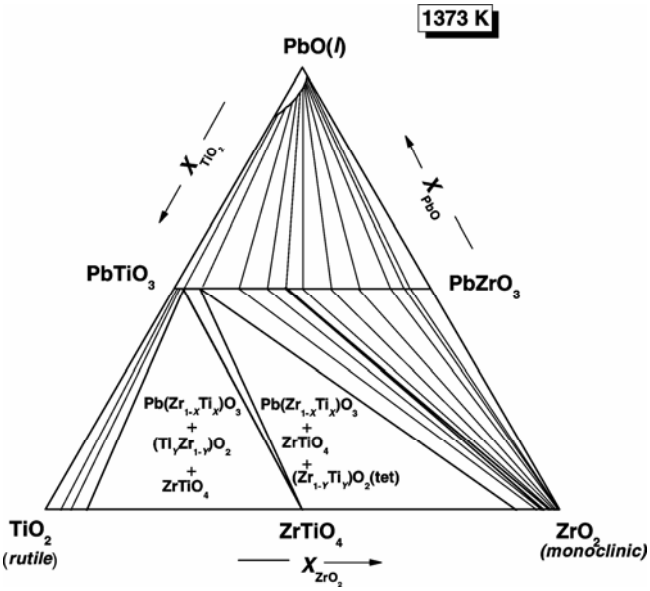

Figure 3. Phase relations in the ternary system PbO–ZrO_2–TiO_2 at 1373 K (Jacob and Rannesh 2007).

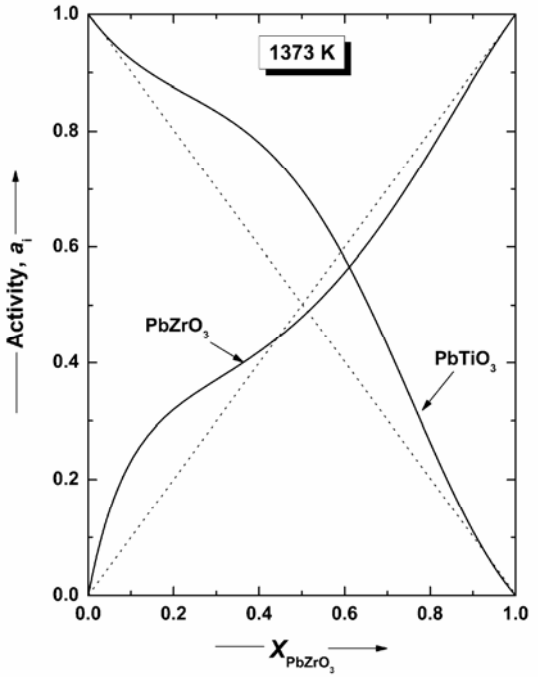

Figure 4. The compositional variation of activities of $PbZrO_3$ and $PbTiO_3$ components in $PbZr_xTi_{1-x}O_3$ solid solution at 1373 K given by Jacob and Rannesh (2007).

Using the same technique, Shim and Jacob (1982) measured the standard Gibbs energy of formation of $PbTiO_3$ from component binary oxides in the temperature range from 1075–1350 K. For the reaction

$$PbO\ (ortho) + TiO_2\ (rut) \rightarrow PbTiO_3\ (cubic), \quad (5)$$

$$\Delta G_5^0\ (\pm 1200)/\text{J mol}^{-1} = -32510 - 0{\cdot}995T. \quad (6)$$

These values show that lead titanate ($PbTiO_3$) is more stable than lead zirconate ($PbZrO_3$) relative to their component binary oxides at all temperatures of interest to PZT and device processing. More recently, Jacob *et al* (2007) reported values for the standard Gibbs energy of formation of $Pb_2Ru_2O_{6\cdot5}$ with pyrochlore structure from PbO, RuO_2 and O_2 in the temperature range from 873–1123 K

$$2PbO\ (ortho) + 2RuO_2\ (rut) + 0{\cdot}25\ O_2\ (g) \rightarrow Pb_2Ru_2O_{6\cdot5}\ (pyro), \quad (7)$$

$$\Delta G_7^0\ (\pm 524)/\text{J mol}^{-1} = -80224 + 75{\cdot}763T - 5{\cdot}873T \ln T. \quad (8)$$

From precise determination of tie-line compositions of $Pb(Zr_xTi_{1-x})O_3$ and $Zr_yTi_{1-y}O_2$ solid solutions at 1373 K, activity–composition relations in $Pb(Zr_xTi_{1-x})O_3$ solid solution, displayed in figure 4, were obtained (Jacob and Rannesh 2007). The activity coefficients of $PbTiO_3$ and $PbZrO_3$ at 1373 K in the solid solution with cubic structure, for the complete range of composition, can be represented by the equations based on Hardy's sub regular solution model (Hardy 1953)

$$\ln \gamma_{PbTiO_3} = 2{\cdot}8505(1 - X_{PbTiO_3})^2 - 3{\cdot}024(1 - X_{PbTiO_3})^3, \quad (9)$$

$$\ln \gamma_{PbZrO_3} = -1{\cdot}685(1 - X_{PbZrO_3})^2 + 3{\cdot}024(1 - X_{PbZrO_3})^3, \quad (10)$$

where the activity coefficient (γ_i) of component i in the solution is defined as the ratio of the activity to mole fraction; $\gamma_i = a_i / X_i$.

Using high-temperature electrochemical method, the activity of TiO_2 in the ZrO_2-rich solid solutions with monoclinic and tetragonal structures in the system ZrO_2–TiO_2 was measured at 1373 K (Jacob *et al* 2006). The activity coefficient of ZrO_2 was derived using the Gibbs–Duhem equation. The following equations represent the results.

For monoclinic structure, in the compositional range $0 \le X_{TiO_2} \le 0{\cdot}02$,

$$\ln \gamma_{TiO_2} = 3{\cdot}145(1 - X_{TiO_2})^2 - 0{\cdot}338, \quad (11)$$

$$\ln \gamma_{ZrO_2} = 3{\cdot}145(X_{TiO_2})^2. \quad (12)$$

For tetragonal structure, in the range $0{\cdot}03 \le X_{TiO_2} \le 0{\cdot}085$,

$$\ln \gamma_{TiO_2} = 2{\cdot}354(1 - X_{TiO_2})^2 + 0{\cdot}064, \quad (13)$$

$$\ln \gamma_{ZrO_2} = 2{\cdot}354(X_{TiO_2})^2 + 0{\cdot}0094. \quad (14)$$

3. Outline of thermodynamic computation

The purpose of the computation is to map the conditions under which PZT solid solutions will react with RuO_2 to form lead ruthenate ($Pb_2Ru_2O_{6{\cdot}5}$). The reaction of each component of the PZT solid solution with RuO_2 can be represented by the following equations

$$2PbZrO_3 + 2RuO_2 + 0{\cdot}25O_2 \rightarrow Pb_2Ru_2O_{6{\cdot}5} + 2ZrO_2, \quad (15)$$

$$\Delta G^0_{15}(\pm 1680)/\text{J·mol}^{-1} = \Delta G^0_7 - 2\Delta G^0_3 = -71144 + 89{\cdot}283T - 5{\cdot}873T\ln T, \quad (16)$$

$$2PbTiO_3 + 2RuO_2 + 0{\cdot}25O_2 \rightarrow Pb_2Ru_2O_{6{\cdot}5} + 2TiO_2, \quad (17)$$

$$\Delta G^0_{17}(\pm 2460)/\text{J·mol}^{-1} = \Delta G^0_7 - 2\Delta G^0_5 = -15204 + 77{\cdot}753T - 5{\cdot}873T\ln T. \quad (18)$$

The standard Gibbs energy changes for (15) and (17) are listed in table 1 for temperatures varying from 600–1400 K. It is seen that the Gibbs energy change for (15) is negative, while that for (17) is positive. Thus, $PbZrO_3$ will react with RuO_2, whereas $PbTiO_3$ will not. The driving force for (15) decreases significantly with temperature. Hence the reaction can be suppressed by increasing temperature. The formation of $Pb_2Ru_2O_{6{\cdot}5}$ according to (15) can also be prevented by reducing the oxygen partial pressure.

In PZT solid solutions, $PbZrO_3$ component will react with RuO_2 resulting in a change of composition of the PZT solid solution and the formation of product phases, $Pb_2Ru_2O_{6{\cdot}5}$ and ZrO_2-rich solid solution containing dissolved TiO_2.

3.1 *Reaction domain at 1373 K*

Presented in this section is the computation of the domain of composition and oxygen partial pressure in which RuO_2 will react with PZT to form lead ruthenate. For convenience, (15) can be rewritten in a modified form as

$$2(PbZrO_3)_{PZT} + 2RuO_2 + 0{\cdot}25O_2 \rightarrow Pb_2Ru_2O_{6{\cdot}5} + 2(ZrO_2)_{ss}. \quad (19)$$

The reactant and product phases, which are present as components of solid solutions, are explicitly identified. The standard Gibbs energy change for (15) and (19) are identical. For a reaction at equilibrium, $\Delta G^0 = -RT\ln K$, where ΔG^0 is the standard Gibbs energy change and K the equilibrium constant for the reaction. Thus

$$\Delta G^0_{19} = \Delta G^0_{15} = -RT\ln K = -RT\ln\left(\frac{(a_{ZrO_2})^2}{P_{O_2}^{0{\cdot}25}(a_{PbZrO_3})^2}\right). \quad (20)$$

Since there is negligible solid solubility of RuO_2 in PZT and ZrO_2 solid solutions, a_{ZrO_2} and a_{PbZrO_3} appearing in (20) are the activities along the tie-lines in the ternary system PbO–TiO_2–ZrO_2, an isothermal section of which at 1373 K is shown in figure 3. The tie-lines connect the composition of PZT solid solution in equilibrium with ZrO_2 solid solution. From the measured tie-line compositions shown in the figure, the activities can be computed using (10) for the activity coefficient of $PbZrO_3$, and (12) and (14) for the activity coefficient of ZrO_2 in monoclinic and tetragonal solid solution phases. From the known standard Gibbs energy change for the reaction, the equilibrium oxygen partial pressure (P_{O_2}) in atmospheres can be computed for tie-line compositions of the PZT solid solution. The relation between P_{O_2} and composition of the PZT solid solution satisfying (20) at 1373 K is displayed in figure 5. Along the curve four condensed phases are in equilibrium with a gas phase. Application of the phase rule to the five-component system indicates that at constant temperature there is one degree of freedom. Either the composition of any one solid solution or oxygen partial pressure can be varied independently. All other parameters are then uniquely defined. In the region above the curve the reaction will occur and the region below is a no reaction zone. It is seen from the plot that only $PbZrO_3$-rich compositions of PZT solid solution will react with RuO_2 at 1373 K. Most of the PZT compositions used in devices will not react with RuO_2 at 1373 K. Decreasing the oxygen partial pressure in the ambient atmosphere will suppress the reaction. The error bars result from uncertainties in the thermodynamic data used for computation. The curve shown in figure 5 can also be computed using standard Gibbs energy change for (17) and activity of $PbTiO_3$ in the PZT solid solution and activity of TiO_2 in ZrO_2 solid solution at compositions defined by tie-lines. Because of the larger uncertainty associated with Gibbs energy change for this reaction (18), the error bars on computed compositions would also be larger.

3.2 *Reaction domain at 1173 K*

The stability domains of $Pb_2Ru_2O_{6{\cdot}5}$ at lower temperatures can be computed using the same procedure. However, tie-line compositions in the ternary system PbO–TiO_2–ZrO_2 have been measured only at 1373 K, and are not available in the literature for lower temperatures. The

Table 1. Standard Gibbs energy changes associated with lead ruthenate formation reactions at different temperatures.

	ΔG^0 (kJ·mol^{-1})				
Reaction	600 K	800 K	1000 K	1200 K	1400 K
Reaction (15)	–40·116	–31·125	–22·430	–13·972	–5·711
Reaction (17)	8·906	15·591	21·980	28·132	34·087

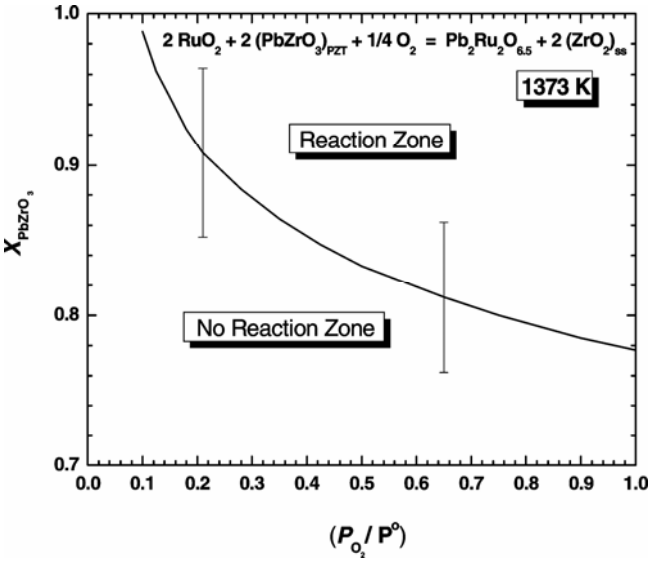

Figure 5. The variation of mole fraction of $PbZrO_3$ in $PbZr_xTi_{1-x}O_3$ in cubic perovskite solid solution as a function of the partial pressure of oxygen at 1373 K for equilibrium between four condensed phases. P^0 is the standard atmospheric pressure; the ratio of pressures is dimensionless with the numerical value equal to the pressure in atmospheres.

tie-lines at lower temperatures can be calculated from the standard Gibbs energies of formation of the compounds and activities in the solid solutions. Thermodynamic data for compounds are available as a function of temperature. However, the activity data are available only at 1373 K. A reasonable estimate of activities at lower temperatures can be obtained if the solution is assumed to have a statistically random distribution of atoms on the substituting site of the solid solution. For a system exhibiting a complete range of solid solubility, if the entropy of cation mixing is ideal, the partial excess Gibbs energy of mixing is independent of temperature, and activity coefficients of a component (γ_i) at constant composition (X_i) at two temperatures T_1 and T_2 are related by the expression

$$[T_1 \ln(\gamma_i)_{T_1}]_{X_i} = [T_2 \ln(\gamma_i)_{T_2}]_{X_i}. \quad (21)$$

This equation is used to compute activity coefficients and hence activities of components of the PZT solid solution at 1173 and 973 K. To estimate activities in ZrO_2-rich ZrO_2–TiO_2 solid solutions with monoclinic and tetragonal structures, Gibbs energy associated with structure transformations have to be considered. The estimated activities at 1173 K are shown as a function of composition in table 2. The standard state for ZrO_2 is the pure oxide with monoclinic structure; for TiO_2 pure rutile form of the oxide.

The tie-lines connecting $Pb(Zr_xTi_{1-x})O_3$ and $Zr_yTi_{1-y}O_2$ solid solutions are governed by the intercrystalline ion exchange reaction (Jacob and Rannesh 2007)

$$(PbZrO_3)_{PZT} + (TiO_2)_{ss} \leftrightarrow (PbTiO_3)_{PZT} + (ZrO_2)_{ss}, \quad (22)$$

$$\Delta G^0_{22}(\pm 1440)/\text{J·mol}^{-1} = \Delta G^0_5 - \Delta G^0_3$$

$$= -27970 + 5{\cdot}765T = RT \ln \frac{a_{PbZrO_3} \cdot a_{TiO_2}}{a_{PbTiO_3} \cdot a_{ZrO_2}}. \quad (23)$$

To compute a tie-line, composition of one of the phases is chosen and the ratio of activities in this phase is computed using the available activity data—measured or estimated—for the phase. From (23) ratio of activities in the second phase can be computed. From this ratio the composition of the second phase can be obtained when activity–composition relations in the second phase are known. The tie-lines at 1173 K derived using this method are displayed in figure 6 using rectangular coordinates for better resolution, rather than the Gibbs triangle representation of phase relations (figure 3). The tie-lines become more skewed with decreasing temperature.

The tie-line data are then used to compute the stability domain of $Pb_2Ru_2O_{6\cdot5}$ as a function of PZT composition and oxygen partial pressure at 1173 K. Displayed in figure 7 are the results obtained. Considerably enlarged is the stability domain of $Pb_2Ru_2O_{6\cdot5}$ compared to the corresponding situation at 1373 K (figure 5).

3.3 *Reaction domain at 973 K*

Following an almost identical procedure for calculations as at 1173 K, the stability domain map at 973 K is obtained (figure 8). At this temperature all the PZT compositions of commercial interest will react with RuO_2 to form lead ruthenate and ZrO_2-rich solid solution unless oxygen partial pressure is substantially reduced.

3.4 *Quaternary representation of phase relations*

Phase relations involving oxide phases in the quinary system Pb–Zr–Ti–Ru–O can be approximated as quater-

nary system PbO–ZrO_2–TiO_2–RuO_2 and displayed in an equilateral tetrahedron, the edges representing the six binaries and the triangular faces representing the four ternary systems. The composition, $Pb_2Ru_2O_{6.5}$, cannot be strictly placed on the binary edge PbO–RuO_2, its location is approximated by a binary point with the same Pb/Ru ratio. The phase relations in the quaternary system at 1173 K and oxygen partial pressure, $P_{O_2}/P^0 = 0{\cdot}21$, is shown in figure 9. Under the specified conditions there is a four-phase equilibrium involving the condensed phases of ZrO_2 (monoclinic solid solution), $PbZr_{0.6}Ti_{0.4}O_3$, $Pb_2Ru_2O_{6.5}$ and RuO_2 corresponding to (19). This four-phase equilibrium is represented by a tie-tetrahedron with the four phases as corners. RuO_2 is not in equilibrium with PZT solid solutions richer in PZ ($PbZr_xTi_{1-x}O_3$; $x > 0{\cdot}6$). As shown in figure 9, the marked plane (tie-triangle) representing ZrO_2 (mono) + $PbZr_{0.6}Ti_{0.4}O_3$ + $Pb_2Ru_2O_{6.5}$ intercepts the line joining RuO_2 to $PbZr_xTi_{1-x}O_3$ with $x > 0{\cdot}6$. PZT solid solutions in this range are equilibrium with $Pb_2Ru_2O_{6.5}$.

Table 2. Activities of TiO_2 and ZrO_2 components as a function of composition in ZrO_2–TiO_2 solid solution at 1173 K.

X_{ZrO_2}	X_{TiO_2}	Structure	a_{ZrO_2}	a_{TiO_2}
1·00	0·00	↑	1·000	0·000
0·99	0·01	Monoclinic	0·990	0·171
0·98	0·02	↓	0·981	0·317
0·97	0·03		0·973	0·443
0·96	0·04	Monoclinic + tetragonal	0·966	0·550
0·91	0·09		0·966	0·550
0·89	0·11	↑	0·955	0·608
0·88	0·12	Tetragonal	0·950	0·631
0·86	0·14	↓	0·942	0·668
0·85	0·15		0·939	0·682
0·84	0·16		0·936	0·694

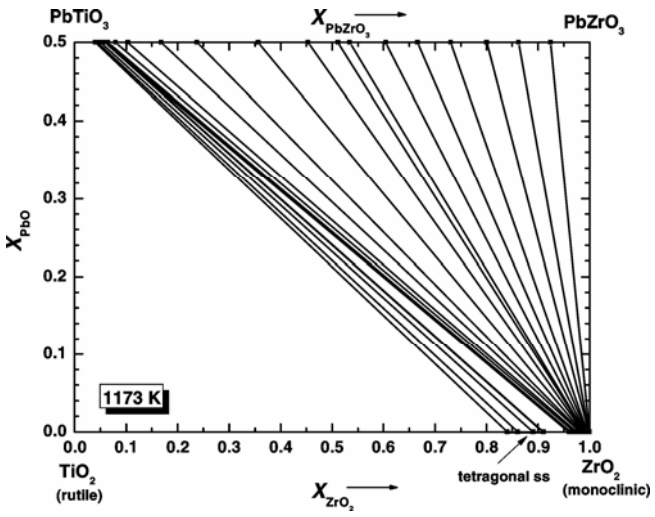

Figure 6. Computed tie-lines between $PbZr_xTi_{1-x}O_3$ solid solution and $Zr_yTi_{1-y}O_2$ solid solutions with monoclinic and tetragonal structures at 1173 K.

3.5 *Application to thin films and nanomaterials*

The computed phase diagrams for the quinary system Pb–Zr–Ti–Ru–O developed in this study delineate the regions where either RuO_2 or $Pb_2Ru_2O_{6.5}$ are stable in contact with PZT solid solutions. The processing conditions such as temperature and oxygen partial pressure can be selected to obtain the desired phase in contact with PZT of

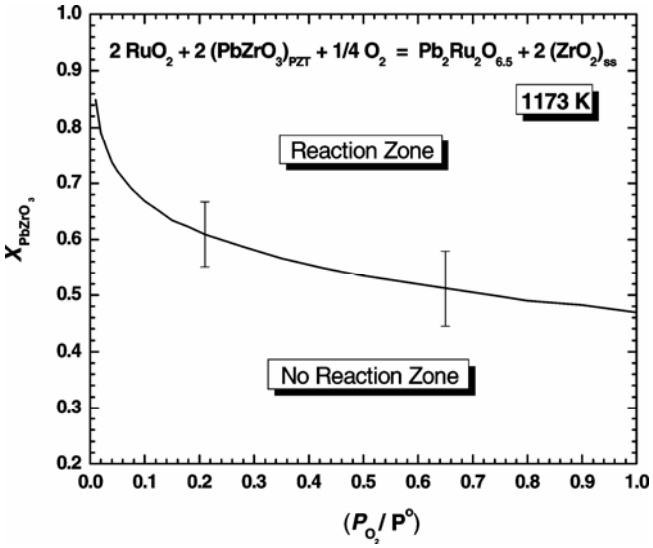

Figure 7. The variation of mole fraction of $PbZrO_3$ in $PbZr_xTi_{1-x}O_3$ in cubic perovskite solid solution as a function of (P_{O_2}/P^0) at 1173 K for (19).

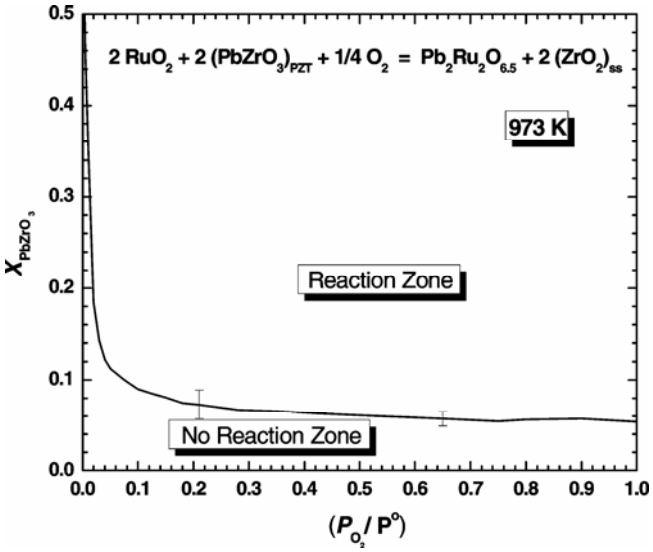

Figure 8. Variation of the mole fraction of $PbZrO_3$ in PZT solid solution as a function of (P_{O_2}/P^0) at 973 K for equilibrium involving four condensed phases.

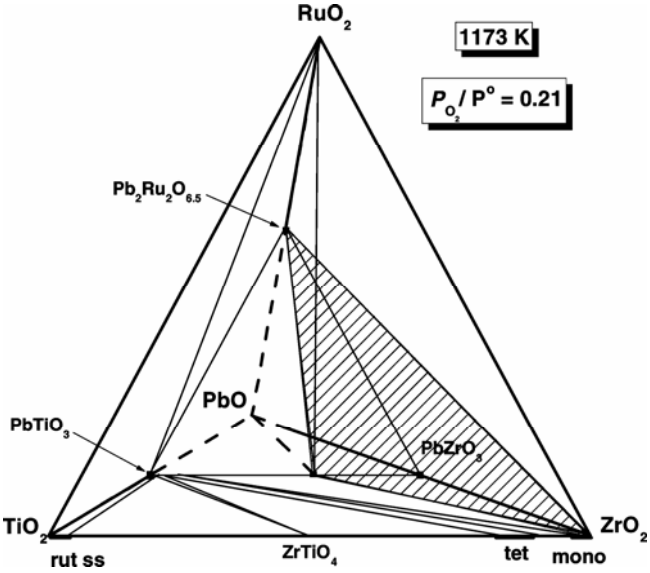

Figure 9. Representation of phase relations in the pseudo-quaternary system PbO–ZrO_2–TiO_2–RuO_2 at 1173 K and $P_{O_2}/P^0 = 0{\cdot}21$.

defined composition. The computations are based on available thermodynamic data for compounds and solid solutions and consistent with currently known phase relations in the subsystems. The computed phase diagram is strictly valid for microcrystalline ceramic samples. When the size of a crystalline phase is reduced in one or more dimensions to the nano range, the Gibbs energies of the crystal will increase. Quantitative measurement of the increase in Gibbs energy at high temperatures is available only for nanocrystalline $MgAl_2O_4$ (Jacob *et al* 2000b). The increase in Gibbs energy in nano-dimensional materials will affect phase relations. Consequently, some shift in phase boundaries is expected in thin film and nanocrystalline samples. Nevertheless, the results presented here provide guidelines for adjusting process parameters to obtain a desired result. The dependence of phase boundaries on oxygen partial pressure and temperature will have more universal validity.

4. Conclusions

Because of its good electrical conductivity, RuO_2 is used as bottom electrode in PZT thin film ferroelectric devices. Under certain conditions, RuO_2 reacts with PZT to form pyrochlore $Pb_2Ru_2O_{6\cdot5}$, which deteriorates the ferroelectric properties of PZT. Although the specific conductivity of $Pb_2Ru_2O_{6\cdot5}$ is approximately seven times lower than that of RuO_2, it has sufficient conductivity to function as an electrode. The choice of RuO_2/Pt and $Pb_2Ru_2O_{6\cdot5}$/Pt hybrid electrodes depends on the specific application. In the present work, the stability fields of RuO_2 and $Pb_2Ru_2O_{6\cdot5}$ in contact with PZT have been computed as a function of processing conditions such as temperature, composition of PZT solid solution and oxygen partial pressure. The computations rely on recently determined standard Gibbs free energy of formation of RuO_2, $Pb_2Ru_2O_{6\cdot5}$ and activities of components of the PZT solid solution. The results indicate that $PbZrO_3$-rich compositions are more prone to react with RuO_2 to form $Pb_2Ru_2O_{6\cdot5}$ at all temperatures. The reaction can be suppressed by increasing temperature and lowering the oxygen partial pressure in the ambient atmosphere.

Acknowledgements

One of the authors (KTJ) is grateful to the Indian National Academy of Engineering, New Delhi, for the award of INAE Distinguished Professorship. (GR) thanks the University Grants Commission of India for the award of Dr D S Kothari Postdoctoral Fellowship.

References

Al-Shareef H N, Bellur K R, Auciello O and Kingon A I 1995 *Thin Solid Films* **256** 73

Bencan A, Hrovat M, Holc J and Kosec M 2001 *J. Eur. Ceram. Soc.* **21** 1451

Hardy H K 1953 *Acta Metall.* **1** 202

Hrovat M, Holc J and Kolar D 1994 *J. Mater. Sci. Letts* **13** 1406

Hrovat M, Bencan A, Holc J and Kosec M 2001 *J. Mater. Sci. Letts* **20** 2005

Ikeda T, Okano T and Watanabe M 1962 *Jpn. J. Appl. Phys.* **1** 218

Jacob K T and Shim W W 1981 *J. Am. Ceram. Soc.* **64** 573

Jacob K T and Rannesh L 2007 *Mater. Sci. & Engg.* **B140** 53

Jacob K T and Subramanian R 2007 *J. Mater. Sci.* **42** 2521

Jacob K T, Mishra S and Waseda Y 2000a *J. Am. Ceram. Soc.* **83** 1745

Jacob K T, Jayadevan K P, Mallya R M and Waseda Y 2000b *Adv. Mater.* **12** 440

Jacob K T, Saji V S and Waseda Y 2006 *High Temp. Mater. Process* **25** 203

Kim S T, Kim H H, Lee M Y and Lee W J 1997 *Jpn. J. Appl. Phys.* **36** 294

Kim S H, Hong J G, Streiffer S K and Kingon A I 1999 *J. Mater. Res.* **14** 1018

Law C W, Tong K Y, Li J H and Poon M C 1999 *Thin Solid Films* **354** 162

Park Y, Jeong S M, Moon S I, Jeong K W, Kim S H, Song J T and Yi J 1999 *Jpn. J. Appl. Phys.* **38** 6801

Seong N J, Choi K J and Yoon S G 2004 *Thin Solid Films* **468** 100

Shim W W and Jacob K T 1982 *Can. Metall. Quart.* **21** 171

Taylor D J, Larsen P K, Dormans G J and Veirman A E 1995 *Integr. Ferroelectr.* **7** 123